Implementing supersymmetric dynamics in ultracold-atom systems

M. Lahrz,[1,2] C. Weitenberg,[2,3] and L. Mathey[1,2,3,*]
[1]*Zentrum für Optische Quantentechnologien, Universität Hamburg, 22761 Hamburg, Germany*
[2]*Institut für Laserphysik, Universität Hamburg, 22761 Hamburg, Germany*
[3]*The Hamburg Centre for Ultrafast Imaging, Luruper Chaussee 149, Hamburg 22761, Germany*
(Received 21 March 2017; published 24 October 2017)

Supersymmetric systems derive their properties from conserved supercharges which form a supersymmetric algebra. These systems naturally factorize into two subsystems, which, when considered as individual systems, have essentially the same eigenenergies, and their eigenstates can be mapped onto each other. We propose a Mach-Zehnder interference experiment to detect supersymmetry in quantum-mechanical systems, which can be realized with current technology. To demonstrate this interferometric technique, we first propose a one-dimensional ultracold-atom setup to realize a pair of supersymmetric systems. Here, a single-atom wave packet evolves in a superposition of the subsystems and gives an interference contrast that is sharply peaked if the subsystems form a supersymmetric pair. Second, we propose a two-dimensional setup that implements supersymmetric dynamics in a synthetic gauge field.

DOI: 10.1103/PhysRevA.96.043624

I. INTRODUCTION

Supersymmetry (SUSY) was originally introduced in particle physics beyond the standard model, but its conceptual structure can be applied outside of high-energy theory, giving rise to supersymmetric quantum mechanics [1–3]. Here, the algebraic structure of SUSY relates two Hamiltonians as supersymmetric partner Hamiltonians. They share the same eigenspectrum, except for the ground state possibly, and the corresponding eigenstates can be mapped onto each other. By mapping a seemingly complicated Hamiltonian onto its supersymmetric partner for which the diagonalization is known, an exact diagonalization can be constructed. This concept has been applied to a wide range of physical problems, e.g., the hydrogen problem [4,5], the Fokker-Planck equation [6,7], and the Korteweg-de Vries equation [8,9]. Recent applications have been reported in [10,11].

We propose an interferometric technique to detect supersymmetry between two systems. We discuss two examples for this technique but emphasize that it can be applied to a wide range of physical systems. Both examples are implementations of the SUSY algebra that consists of a Hamiltonian $\mathcal{H}$ and a supercharge operator Q. We assume that these operate on a 2-spinor $\psi = (\psi^{(1)}, \psi^{(2)})$ (see [12]). The supercharge Q is a conserved quantity of $\mathcal{H}$ and fulfills the defining equation $\{Q, Q^\dagger\} = \mathcal{H}$. We choose Q to have the form $Q = \hat{B}\sigma^+$, where σ^+ is the Pauli spin-raising matrix and $\hat{B}$ is a scalar operator. With this, $\mathcal{H}$ takes the form $\mathcal{H} = \hat{H}^{(1)}\mathbf{1}_\uparrow + \hat{H}^{(2)}\mathbf{1}_\downarrow$, with $\mathbf{1}_{\uparrow/\downarrow} = (\mathbf{1} \pm \sigma_z)/2$ and with $\hat{H}^{(1)} = \hat{B}\hat{B}^\dagger$ and $\hat{H}^{(2)} = \hat{B}^\dagger\hat{B}$. So the system separates into two scalar subsystems (see [13]). Considering $\hat{H}^{(1)}$ and $\hat{H}^{(2)}$ as individual Hamiltonians, these are supersymmetric partners. They have the same spectrum, with the possible exception of the ground state of $\hat{H}^{(2)}$, and the operator $\hat{B}$ maps the eigenstates $\psi_n^{(2)}$ of $\hat{H}^{(2)}$ onto the eigenstates $\psi_n^{(1)}$ of $\hat{H}^{(1)}$ [see Fig. 1(a)]. We have $\hat{B}\psi_n^{(2)} \sim \psi_n^{(1)}$, where $\psi_n^{(1)}$ and $\psi_n^{(2)}$ have the same eigenenergy E_n, and similarly, $\hat{B}^\dagger\psi_n^{(1)} \sim \psi_n^{(2)}$. The zero-energy state of $\hat{H}^{(2)}$ is annihilated by $\hat{B}$, i.e., $\hat{B}\psi_0 = 0$, if it exists. This case of unbroken supersymmetry is indeed realized in both examples in this paper. We give an example for broken supersymmetry in Appendix A. The number of zero-energy states is the Witten index and is directly relevant for the proof of the Atiyah-Singer index theorem (Refs. [3,14,15]). As a second realization of this SUSY algebra, we discuss two-dimensional motion of a spin-1/2 particle in a synthetic gauge field [16].

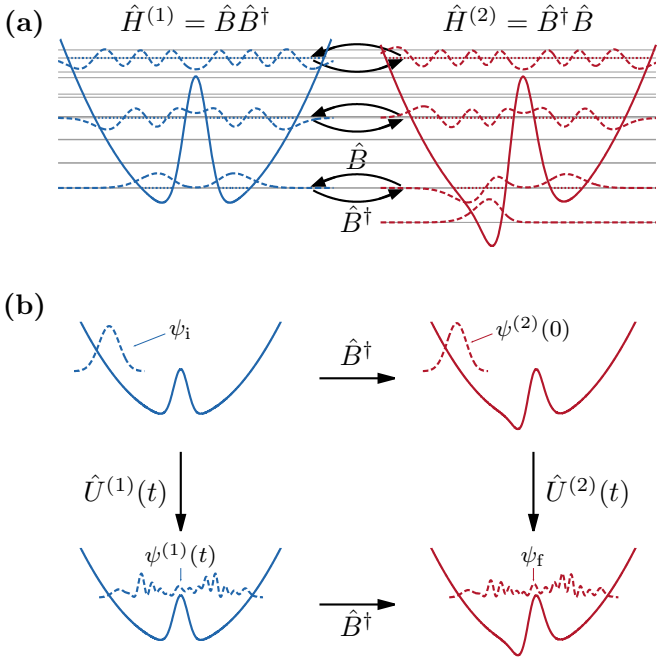

FIG. 1. Supersymmetric partner systems manifest themselves equivalently as follows. (a) The spectra coincide, except for a zero-energy state of $\hat{H}^{(2)}$ for unbroken supersymmetry. Additionally, the eigenstates can be mapped onto each other via $\hat{B}^\dagger$ and $\hat{B}$. (b) The time propagation of each system can be mapped onto each other via $\hat{B}^\dagger$ at any time t.

*Corresponding author: lmathey@physnet.uni-hamburg.de

The supersymmetric relation between two Hamiltonians translates into

$$\hat{B}^\dagger \hat{U}^{(1)}(t) = \hat{U}^{(2)}(t)\hat{B}^\dagger \tag{1}$$

for their time propagators $\hat{U}^{(1/2)}(t) = \exp(-i\hat{H}^{(1/2)}t/\hbar)$ for any time t [see Fig. 1(b)]. $\hbar$ is the reduced Planck constant. We propose to implement and detect the supersymmetric relation of the time propagators in Eq. (1) in an ultracold-atom experiment. To make the experimental realization of the operator $\hat{B}^\dagger$ feasible, we propose to use a trivially supersymmetric system with a supercharge that can be realized experimentally and to adiabatically deform this system into the desired system. Our first example provides an illustration of this proposal. Here, supersymmetric quantum mechanics is realized in the one-dimensional Schrödinger equation. The trivially supersymmetric system is the harmonic oscillator, which is then deformed into a nonharmonic system by adding additional potential barriers. In the second example we discuss atomic motion in a synthetic gauge field in two dimensions. In each case, we consider a single atom subjected to an interferometric protocol, but we emphasize that a similar approach can be taken to higher-dimensional systems or many-body systems.

This paper is organized as follows. In Sec. II we describe the Hamiltonian of our first example of an atom moving in a potential in one dimension. In Sec. III we present our interferometric protocol. In Sec. IV we discuss atomic motion in an artificial gauge field, and in Sec. V we conclude.

II. SUPERSYMMETRY OF THE ONE-DIMENSIONAL SCHRÖDINGER EQUATION

In the first example, the atom initially moves in a one-dimensional harmonic trap potential, as mentioned. The atom is prepared in the ground state and then split coherently, either by spatially splitting the trap in one of the confining directions (see, e.g., Ref. [17]) or by applying a $\pi/2$ pulse to a second internal state, such as a hyperfine state. Then an approximation of $\hat{B}^\dagger$ is applied to the second component of the wave packet (see Fig. 2). Both parts of the wave packet are shifted away from the potential minimum, and for each an additional potential barrier, localized near the harmonic potential minimum, is ramped up. The wave-packet components then move in each of these potentials. They oscillate in the harmonic potential and scatter off the potential barriers. Then $\hat{B}^\dagger$ is applied to the first component of the wave packet, and the two components are brought to interference.

This interferometer probes if the two Hamiltonians $\hat{H}^{(1)}$ and $\hat{H}^{(2)}$, with $\hat{H}^{(i)} = \hat{H}_{\rm kin} + V^{(i)}$, are supersymmetric partners, with $\hat{H}_{\rm kin} = -\hbar^2/(2m)\partial_{xx}$. m is the atom mass. The potentials are $V^{(i)} = V_{\rm osc} + V^{(i)}_{\rm loc}$, with the confining potential $V_{\rm osc} = m\omega^2 x^2/2$, where ω is the trap frequency. The additional potentials $V^{(i)}_{\rm loc}$ fall off on a length scale σ. The initial displacement $\bar{x}$ of the wave packets is such that $\bar{x} \gg \max(x_0, \sigma)$, where x_0 is the harmonic oscillator length, $x_0 = \sqrt{\hbar/(m\omega)}$. In this setup the atom scatters repeatedly off the potential barriers, which strongly increases the interference contrast discussed below, which identifies the supersymmetric relation between the two subsystems. We note that other, nonharmonic confining potentials can also be used (see Appendixes A and B).

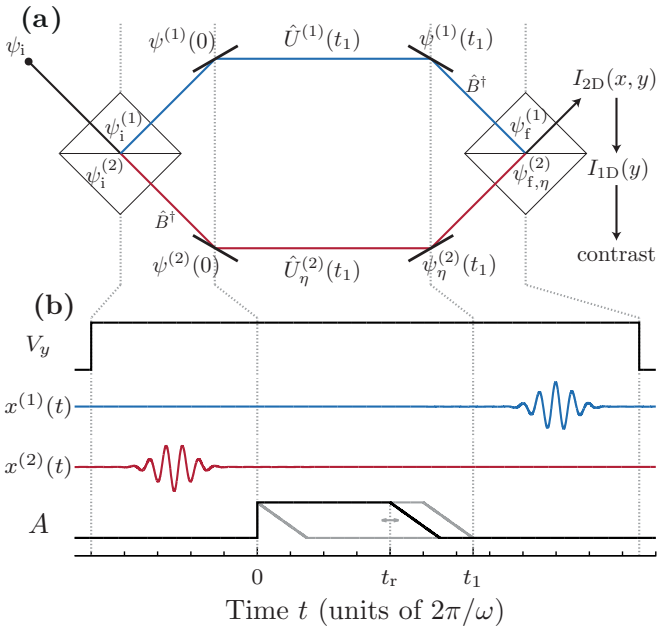

FIG. 2. (a) Mach-Zehnder interferometer. The initial state $\psi_{\rm i}$ is split to evolve along the two paths corresponding to the supersymmetric partners. $\hat{B}^\dagger$ is applied before or after the time evolution, depending on the path. Finally, the paths are brought to interference, resulting in a contrast measurement. (b) Experimental sequence. Assuming the beam splitter is realized by spatial splitting, the potential barrier V_y in the y direction is smoothly turned on and rapidly turned off. $\hat{B}^\dagger$ is approximated by a shaking process. During this shaking, we turn off the nonharmonic potentials, i.e., $A = 0$. A is held at a constant nonzero value for a hold time $t_{\rm r}$ and then ramped down linearly.

As our main example, we consider

$$V^{(i)}_{\rm loc}(x) = V^{(i)}_{\rm s} \exp\left(-\frac{x^2}{2\sigma^2}\right) + V^{(i)}_{\rm p} x \exp\left(-\frac{x^2}{4\sigma^2}\right). \tag{2}$$

Each potential has a Gaussian term, which we refer to as the s barrier, and a term of the form $\sim x\exp[-x^2/(4\sigma^2)]$, which we refer to as the p barrier. The s barrier has a width σ; the p barrier has a width $\sqrt{2}\sigma$.

One approach to realize this potential experimentally is to use a spatial light modulator (see, e.g., Refs. [18–21]), which also allows for selective control of spatially separated potentials close to each other. Alternatively, the s barrier can be realized with a blue-detuned Gaussian beam, which results in a repulsive potential. The p barrier can be realized by using two Gaussian beams, one blue detuned and located at $+x_b$, with $x_b \ll \sigma$, and one red detuned, located at $-x_b$.

Remarkably, in the parameter space of the two potentials in Eq. (2), there is a submanifold for which these two systems are supersymmetric partners. To determine this manifold, we consider the ansatz $\hat{B}^\dagger = [W(x) - \hbar\partial_x/\sqrt{m}]/\sqrt{2}$. $W(x)$ is the superpotential of the system. Using $\hat{H}^{(1)} = \hat{B}\hat{B}^\dagger$ and $\hat{H}^{(2)} = \hat{B}\hat{B}^\dagger$, we obtain $\hat{H}^{(i)} = \hat{H}_{\rm kin} + V^{(i)}$, with $V^{(i)}(x) = W^2(x)/2 \pm \hbar W'(x)/(2\sqrt{m})$. We use $W(x) = \sqrt{\hbar\omega}\{x/x_0 + A\exp[-x^2/(4\sigma^2)]\}$ for the superpotential. The first term creates the harmonic potential; the second term creates the

barrier potentials. A is the dimensionless amplitude of the Gaussian term. This gives

$$V^{(i)}(x) = \frac{m\omega^2 x^2}{2} \mp \frac{\hbar\omega}{2} + \frac{\hbar\omega A^2}{2} \exp\left(-\frac{x^2}{2\sigma^2}\right) + \frac{2\hbar\omega A x}{x_0}\left(1 \mp \frac{x_0^2}{4\sigma^2}\right)\exp\left(-\frac{x^2}{4\sigma^2}\right). \quad (3)$$

Thus the prefactors of the barrier potentials have to fulfill $V_s^{(1/2)} = \hbar\omega A^2/2$ and $V_p^{(1/2)} = 2\hbar\omega A[1 \mp x_0^2/(4\sigma^2)]/x_0$. We choose $\sigma = x_0/2$, resulting in $V_p^{(1)} = 0$ and $V_p^{(2)} = 4\hbar\omega A/x_0$. For $A = 0$, the potentials reduce to $V^{(i)}(x) = V_{\rm osc} \mp \hbar\omega/2$, which is a supersymmetric pair with $\hat{B}^\dagger = \sqrt{\hbar\omega}\hat{a}^\dagger$, with $\hat{a}^\dagger$ being the harmonic oscillator creation operator. We use this pair of potentials as the trivially supersymmetric system which we deform during the interferometric protocol by turning A on and off.

For comparison, we define $V_\eta(x) = V_{\rm osc}(x) + (\hbar\omega A^2/2)\exp(-2x^2/x_0^2) + (2\eta\hbar\omega A x/x_0)\exp(-x^2/x_0^2)$ as a family of potentials parametrized by η. For $\eta = 0$, this is $V^{(1)}(x)$, up to an energy offset, and for $\eta = 1$, $V_\eta(x)$ is $V^{(2)}(x)$. We will depict the interference contrast between the potential for $\eta = 0$ and the potential for arbitrary η. For $\eta = 1$ the response will be strongly peaked, demonstrating the existence of supersymmetry. In Appendix C, the spectrum of $V_\eta(x)$ is shown as a function of η. The isospectral feature at $\eta = 1$ is clearly visible.

III. INTERFEROMETRIC PROTOCOL

In the protocol, initially, we use $A = 0$ [see Fig. 2(b)]. The atom is prepared in the ground state $\chi_0(x) = (\pi x_0^2)^{-1/4}\exp[-x^2/(2x_0^2)]$ (e.g., Ref. [22]) in one of the internal states. Then a coherent superposition in the interferometer paths is created. Next, we displace the wave function in the following example by $\bar{x} = -5\,x_0$ and apply $\hat{B}^\dagger$ to state 2. As mentioned, $\hat{B}^\dagger$ reduces to $\sqrt{\hbar\omega}\hat{a}^\dagger$ for $A = 0$. When we apply $\hat{a}^\dagger$ to the shifted-ground-state wave function, we obtain a superposition of a shifted ground state $\chi_0(x)$ and a shifted first excited state $\chi_1(x)$ of the harmonic oscillator, that is, $\zeta_1\chi_1(x - \bar{x}) + \zeta_0\chi_0(x - \bar{x})$. The amplitudes $\zeta_{0/1}$ depend on $\bar{x}$ and are $\zeta_0^2 = \bar{x}^2/(\bar{x}^2 + 2x_0^2)$ and $\zeta_1^2 = 2x_0^2/(\bar{x}^2 + 2x_0^2)$. For $\bar{x} = -5\,x_0$, this gives $\zeta_0^2 = 49/53$ and $\zeta_1^2 = 4/53$. Thus only a small admixture of the excited state is necessary to implement $\hat{B}^\dagger$ for $\bar{x} \gg x_0$.

To create this admixture, we perform a shaking process of the harmonic trap, i.e., $V^{(2)}(x,t) = V_{\rm osc}[x - x^{(2)}(t)]$ [see Fig. 2(b)]. We choose $x^{(2)}(t) = \delta_x \sin(\Omega t)\tau(t)$, where δ_x is the shaking amplitude; Ω is the shaking frequency, resonant with the trap frequency $\Omega = \omega$; and a Gaussian envelope $\tau(t) = \exp[-(t - t_0)^2/(2\sigma_t^2)]$ with a pulse length σ_t. t_0 is the pulse time, which we choose to be well separated from turning on the barrier potentials at $t = 0$, with $t_0 = -5\sigma_t$. This perturbation is of the form $-F(t)\hat{x}$, with $F(t) = m\omega^2 x^{(2)}(t)$, ignoring an overall energy shift. The $\hat{x}$ operator is $\hat{x} \sim \hat{B}^\dagger + \hat{B}$, which is applied to the ground state, giving a small admixture of the first excited state for a small driving term. In Appendix D we discuss the optimal shaking parameters.

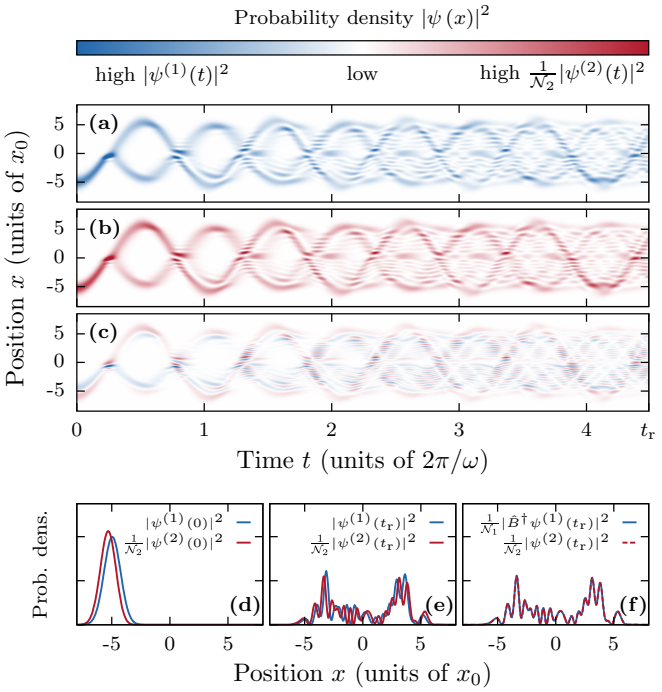

FIG. 3. In (a) and (b) we show $|\psi^{(1)}(x)|^2$ and $|\psi^{(2)}(x)|^2/\mathcal{N}_2$, respectively, and in (c) we show their difference. $|\psi^{(2)}(x)|^2$ was normalized by $\mathcal{N}_2 = (\langle\hat{B}\hat{B}^\dagger\rangle_{2,t=0})^{1/2}$, after $\hat{B}^\dagger$ was applied at $t = 0$, to obtain a probability distribution. In (d) we show the initial densities, and in (e) we show those at time $t_r = 4.5 \times 2\pi/\omega$. In (f) we demonstrate that the two densities coincide after $\hat{B}^\dagger$ has been applied to $\psi^{(1)}(x)$ and normalized by $\mathcal{N}_1 = (\langle\hat{B}\hat{B}^\dagger\rangle_{1,t=t_r})^{1/2}$.

Having applied $\hat{B}^\dagger$ to state 2 and shifted both states by $\bar{x}$, the resulting densities are shown in Fig. 3(d). The barrier potentials are ramped up at $t = 0$. We use $A = \sqrt{26}$ (see [23]). Figures 3(a) and 3(b) show the evolution of the two densities. These differ at any time, which is clearly visible by depicting their difference [Fig. 3(c)], due to the different barriers and initial wave functions. We show $|\psi^{(1)}(x,t_r)|^2$ and $|\psi^{(2)}(x,t_r)|^2/\mathcal{N}_2$ in Fig. 3(e). If we apply $\hat{B}^\dagger$ to state 1, $|\hat{B}^\dagger\psi^{(1)}(x,t_r)|^2/\mathcal{N}_1$ and $|\psi^{(2)}(x,t_r)|^2/\mathcal{N}_2$ coincide [see Fig. 3(f)], demonstrating supersymmetric dynamics.

To implement $\hat{B}^\dagger$, after A has been ramped down and after time t_1, we again perform a shaking pulse, $x^{(1)}(t) = \delta_x \sin(\Omega t)\tau(t)$. $\psi^{(1)}(x,t_1)$ is a superposition of oscillator states that is controlled by the initial displacement $\bar{x}$, which results in $\bar{n} \approx \bar{x}^2/(2x_0^2)$, where $\bar{n}$ is the average occupation number. In contrast to the first shaking process, now both $\hat{B}^\dagger$ and $\hat{B}$ will affect the wave function. Therefore the maximal overlap of the desired and the implemented operator is approximately $1/\sqrt{2}$. This magnitude can indeed be achieved (see Fig. 4). The contribution of $\hat{B}$ to the interference contrast is oscillatory in time and can be removed by time averaging. In Fig. 8 we show the operator that is realized via the shaking process. For the desired energy range, this gives satisfactory agreement with $\hat{B}^\dagger$.

Finally, we bring the two paths to interference (see Appendix E). The interference contrast is

$$\mathcal{C} = \frac{2|\langle\psi_{\rm f}^{(1)}|\psi_{{\rm f},\eta}^{(2)}\rangle|}{\langle\psi_{\rm f}^{(1)}|\psi_{\rm f}^{(1)}\rangle + \langle\psi_{{\rm f},\eta}^{(2)}|\psi_{{\rm f},\eta}^{(2)}\rangle}, \quad (4)$$

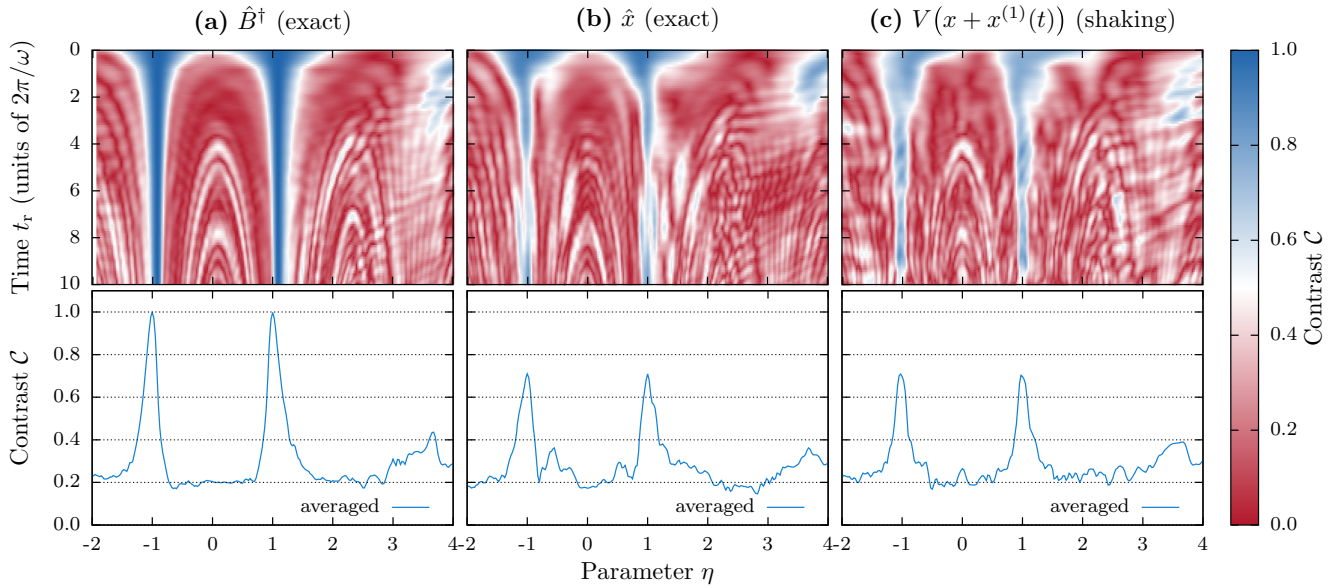

FIG. 4. In the top panels of (a), (b), and (c) we show the contrast as a function of t_r and η. In (c), we interfere $\psi^{(2)}(t_1)$ with $\psi^{(1)}(t_1)$ after the shaking pulse, by applying a $\pi/2$ pulse. For comparison, we show the contrast with $\hat{B}^\dagger\psi^{(1)}(t_1)$ and $\hat{x}\psi^{(1)}(t_1)$ in (a) and (b), respectively, each properly normalized (compare with Fig. 3). The linear ramp-down time of A after t_r is $3 \times 2\pi/\omega$. In the bottom panels, the contrast has been averaged over $t_r = 0, \ldots, 10 \times 2\pi/\omega$. The peaks at $\eta = \pm 1$ demonstrate supersymmetry.

where $\psi_f^{(1)}$ and $\psi_{f,\eta}^{(2)}$ are the states that emerge from the paths [see Fig. 2(a)]. $\mathcal{C}$ is depicted in Fig. 4 as a function of t_r and η in the top panels. We compare the contrast for the exact application of $\hat{B}^\dagger$, the exact application of $\hat{x}$, and the shaking pulse. The latter reproduces the exact pattern well. The lower three panels show the contrast averaged over the hold time t_r. The peaks at $\eta = \pm 1$ demonstrate supersymmetry, as desired [24].

IV. SUPERSYMMETRY IN SYNTHETIC GAUGE FIELDS

The second realization of the SUSY algebra is the Pauli equation

$$\mathcal{H} = \frac{(p_x + A_x)^2}{2m} + \frac{(p_y + A_y)^2}{2m} + V(\mathbf{r}) + \frac{\hbar g}{4m} B_z \sigma_z \qquad (5)$$

in two dimensions for $V(\mathbf{r}) = 0$ and for $g = 2$. The supercharge is $Q^\dagger = -\sigma^+[(p_y + A_y) + i(p_x + A_x)]/(\sqrt{2m})$ (see Refs. [3,25]). Thus, for this unique value of the gyromagnetic ratio g, there exists an additional conserved quantity that mixes orbital and spin motion in an arbitrary vector field $\mathbf{A}$.

In Ref. [26] the synthetic gauge field $A_x = By$ and $A_y = 0$, with $B > 0$, was proposed and realized. This vector potential gives Landau-level dynamics in each spin state described by $H = \omega_c(\pi_x^2 + \pi_y^2 - \hbar\sigma_z)/2 = \hbar\omega_c[a^\dagger a + (1 - \sigma_z)/2]$, where we introduced $\pi_{x,y} = (p_{x,y} + A_{x,y})/\sqrt{B}$. For this linear vector potential, these are canonical variables, $[\pi_x, \pi_y] = i\hbar$, so we define $a = (\pi_x + i\pi_y)/\sqrt{2\hbar}$, which are bosonic operators. $\omega_c = B/m$ is the cyclotron frequency. The cyclotron motion is centered around $\mathbf{R} = (X, Y)$, with $X = x + \pi_y/\sqrt{B}$ and $Y = y - \pi_x/\sqrt{B}$. For $\langle X \rangle = \langle Y \rangle = 0$, the Landau levels are $(a^\dagger)^n\psi_0 \sim \exp(in\phi)\rho^n \exp[-\rho^2/(4\rho_0^2)]$, with $n = 0, 1, 2, \ldots$, $\rho = \sqrt{x^2 + y^2}$, and the magnetic length $r_0 = \sqrt{\hbar/(m\omega_c)}$. The ground state ψ_0 is $\psi_0 \sim \exp[-\rho^2/(4\rho_0^2)]$. We note that these are also the eigenstates of the two-dimensional harmonic oscillator, $H_{\text{osc}} = \mathbf{p}^2/(2m) + m\omega_c^2\mathbf{r}^2/2$, with the same energies $\hbar\omega_c(n + 1/2)$ and with the angular momentum $l_z = n$.

We propose the following protocol to detect and realize supersymmetry of this system. Initially, $\mathbf{A}$ is turned off, and a harmonic potential $V_{\text{osc}}(\mathbf{r}) = m\omega_c^2\mathbf{r}^2/2$ is turned on, which we again use as the trivially supersymmetric system. The atom is prepared in the ground state ψ_0 in the spin state $\uparrow$. A $\pi/2$ pulse is applied, and the $a^\dagger$ operator, operating on $\downarrow$, is implemented by shaking the potential $V_{\text{osc}}[\mathbf{r} - \mathbf{r}_0(t)]$, while the potential of $\uparrow$ is stationary. The circular shaking is given by $\mathbf{r}_0(t) = \delta(x\cos(\Omega t), y\sin(\Omega t))\tau(t)$, with a protocol similar to that for the one-dimensional case, generating approximately the transitions $n \to n + 1$ and $l_z \to l_z + 1$. Then the harmonic potential is ramped down, and the gauge field is ramped up. Remarkably, any gauge field supports supersymmetry. Therefore an arbitrary $\mathbf{A}(\mathbf{r}, t)$ can be used in the interferometric paths, preserving $\langle X \rangle = \langle Y \rangle = 0$, with the final states $A_x = By$ and $A_y = 0$ again. Then $\mathbf{A}$ is switched off, and the harmonic potential is switched on. The circular shaking process is applied to the state $\uparrow$, and a $\pi/2$ pulse is used to bring the paths to interference. To detune the system away from supersymmetry, either a potential $V(\mathbf{r}) \neq 0$ can be applied, or g can be tuned as $g = 2\eta$. Then, a peak at $\eta = \pm 1$ demonstrates supersymmetry.

V. CONCLUSIONS

In this paper we have demonstrated an interferometric method to realize and detect supersymmetric dynamics in ultracold-atom systems, realizable with current technology. To illustrate this general interferometric method, we have presented two examples which both realize a supersymmetric algebra with one supercharge. The first consists of one-dimensional motion in a pair of potentials; the second

consists of two-dimensional motion of an atom in a synthetic gauge field. We have given a detailed description of the experimental sequence, including a beam-splitter step, the application of the supercharge operator, and the constraints on the Hamiltonians of the two subsystems. We used the first example to demonstrate that this protocol gives a sharp interference peak if the system is supersymmetric.

From a practical perspective, an intriguing application is a case in which a supersymmetric partner of a desired system is technically easier to realize than the original system, such as the box potential for which we show its supersymmetric partner in Fig. 6(c). Instead of the technically more challenging box potential, the supersymmetric mapping on its isospectral partner potential can be implemented by first applying $\hat{B}^\dagger$, letting the system evolve under its smooth and experimentally feasible partner system, and then applying $\hat{B}$, which gives a state identical to the one that emerges under time evolution of the original system.

More conceptually, the existence of conserved supercharges and the supersymmetric algebraic structure provide a fresh perspective on dynamics in synthetic gauge fields. Finally, these concepts could potentially be used to test extensions of the Atiyah-Singer index theorem on manifolds with open boundaries by creating gauge fields that constrain the motion of a particle to a nontrivial topological subset of the two-dimensional plane.

ACKNOWLEDGMENTS

We acknowledge support from the Deutsche Forschungsgemeinschaft through the SFB 925 and the Hamburg Centre for Ultrafast Imaging and from the Landesexzellenzinitiative Hamburg, which is supported by the Joachim Herz Stiftung.

APPENDIX A: BROKEN AND UNBROKEN SUPERSYMMETRY

For a pair of supersymmetric Hamiltonians with unbroken supersymmetry, there exists a zero-energy state $\psi_0^{(2)}$ in the system described by the Hamiltonian $\hat{H}^{(2)} = \hat{B}^\dagger\hat{B}$, which is annihilated by the operator $\hat{B}$, i.e., $\hat{B}\psi_0^{(2)} = 0$. It can be expressed in terms of the superpotential $W(x)$, that is, $\psi_0^{(2)} \sim \exp[\sqrt{m}\Omega(x)/\hbar]$, with $\Omega(x) = \int^x W(u)du$. For the wave function $\psi_0^{(2)}(x)$ to be normalizable, it has to fall off to zero for $|x| \to \infty$. Therefore, the superpotential must fulfill $W(x \to \pm\infty) = \pm\infty$. An example for unbroken supersymmetry is the one-dimensional case presented in this paper, with the zero-energy state of $\hat{H}^{(2)}$ visible on the right in Fig. 1(a).

For supersymmetric Hamiltonians with broken supersymmetry, no zero-energy state exists. All eigenstates have a partner state. To give an example for broken supersymmetry, we choose the superpotential as follows:

$$W(x) = \sqrt{2\hbar\omega}\left[\frac{x^2}{x_1^2} + c\tanh\left(\frac{x}{x_2}\right)\right], \tag{A1}$$

where x_1 and x_2 are characteristic length scales and c is a dimensionless constant. Note that $W(x \to \pm\infty) = \infty$, which breaks the supersymmetry. Furthermore, $W(x) \neq W(-x)$ to avoid the trivial case of $V^{(1)}(x) = V^{(2)}(-x)$. The supersymmetric potentials are then given by

$$V(x)^{(1/2)} = \hbar\omega\left\{\left[\frac{x^2}{x_1^2} + c\tanh\left(\frac{x}{x_2}\right)\right]^2 \pm\sqrt{\frac{\hbar}{2m\omega}}\left[\frac{2x}{x_1^2} + \frac{c}{x_2}\,\mathrm{sech}^2\left(\frac{x}{x_2}\right)\right]\right\}, \tag{A2}$$

where the upper sign is for $V^{(1)}$ and the lower sign is for $V^{(2)}$. We show an example of this family of supersymmetric potentials in Fig. 5.

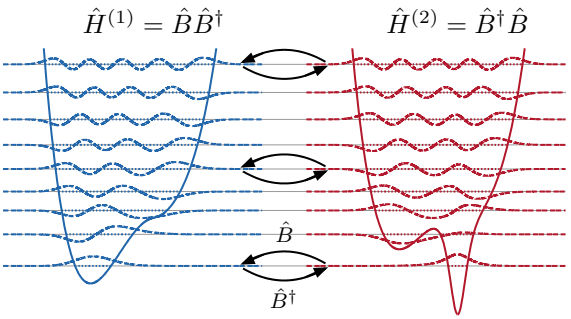

FIG. 5. Example of a pair of potentials with broken supersymmetry [see Eq. (A2)], with $x_1 = 2$, $x_2 = 1/2$, and $c = 2$. $\hat{H}^{(2)}$ does not have an additional zero-energy state; all states have a partner state.

APPENDIX B: NONHARMONIC CONFINING POTENTIALS

In our main example for supersymmetric quantum mechanics in one dimension, we considered a linear term in the superpotential and thus harmonic confinement in the potentials $V^{(1)}$ and $V^{(2)}$. This linear term by itself gives the potentials $V^{(1)} = V_{\mathrm{osc}}$ and $V^{(2)} = V_{\mathrm{osc}} + \hbar\omega$, which are supersymmetric partners. Here, we give two examples in which these potentials have a confining potential that is not harmonic in addition to the example in the previous section.

As a first example, we consider a superpotential of the form $W(x) = cx^n$, where c is a constant and n is a positive integer. The potentials are $V^{(1/2)}(x) = c^2x^{2n} \mp cnx^{n-1}$ and approach each other asymptotically in the limit $x \to \infty$. If n is even, the isospectral character of the supersymmetric partners is trivial since $V^{(1)}(x) = V^{(2)}(-x)$. If n is odd, one of the potentials, depending on the sign of c, has a double-well structure with a local maximum at $x = 0$ while the other has a single minimum at $x = 0$. We show examples for $n = 2$ and $n = 3$ in Figs. 6(a) and 6(b).

As a second example we consider the box potential $V^{(1)}(x) = -\pi^2$ for $0 < x < 1$ and infinity otherwise. The supersymmetric partner is $V^{(2)}(x) = \pi^2[2\sin^{-2}(\pi x) - 1]$ for $0 < x < 1$, softening the singularities at the edges of the box [see Fig. 6(c)].

APPENDIX C: SPECTRUM OF THE POTENTIAL $V_\eta(x)$

We determine the spectra of $V_\eta(x)$ as a function of η and compare them to the spectrum of $V_{\eta=0}(x) + \hbar\omega$ (see Fig. 7). The spectra of $V_{\eta=1}(x) = V^{(2)}(x)$ and $V_{\eta=0}(x) +$

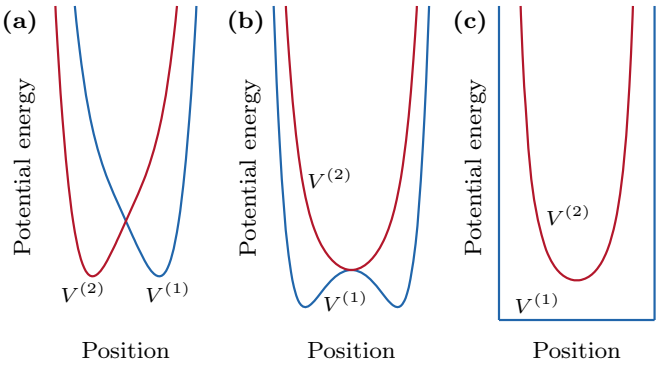

FIG. 6. Examples of nonharmonic supersymmetric confining potentials. (a) $V^{(1/2)}(x) = 0.01x^4 \mp 0.2x$. (b) $V^{(1/2)}(x) = 0.01x^6 \mp 0.3x^2$. (c) Box potential $V^{(1)}$ and $V^{(2)} = \pi^2[2\sin^{-2}(\pi x) - 1]$.

$\hbar\omega = V^{(1)}(x)$ coincide, except for an additional ground state, indicating the unbroken supersymmetric relation at this point.

APPENDIX D: OPTIMAL SHAKING PARAMETERS

We approximate the operator $\hat{B}^\dagger$ with a shaking process (see Fig. 2) of the harmonic potential of the form $V(x,t) = V_{\rm osc}[x + x(t)]$, where $x(t) = \delta_x \sin(\Omega t + \phi)\tau(t)$, with the shaking amplitude δ_x, the carrier frequency of the shaking Ω, and the phase of the driving ϕ. We fix the carrier frequency to $\Omega = \omega$ to be on resonance. We use a Gaussian envelope $\tau(t) = \exp[-(t-t_0)^2/(2\sigma_t^2)]$ of width σ_t, where $t_0 = -5\sigma_t$ is the center of the pulse driving from $t = -10\sigma_t$ to 0.

Based on a path-integral ansatz for the forced harmonic oscillator [27], we have analytic access to the transition matrix elements in the Fock basis, $T_{mn} = \langle m|\hat{U}(t)|n\rangle$ [see Fig. 8(a)]. In particular, the transition amplitude from the ground state

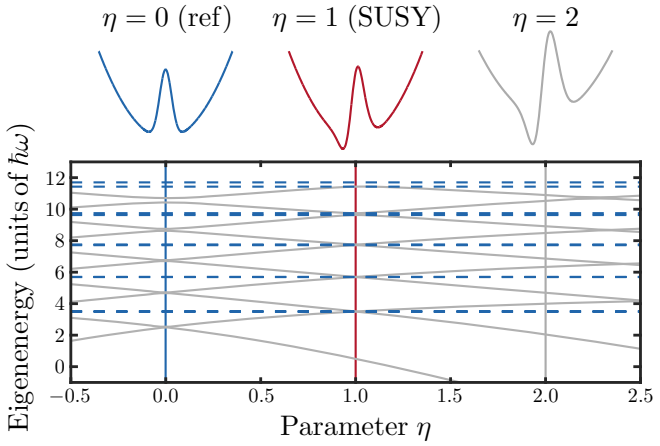

FIG. 7. Spectrum of $V_\eta(x)$ as a function of η (solid gray curves) compared to the spectrum of the reference $V^{(1)}(x)$ (dashed blue curves). The positions of the reference ($\eta = 0$), its supersymmetric partner ($\eta = 1$), and an arbitrary nonsupersymmetric case ($\eta = 2$) are marked. The crossing of the dashed blue curves with the gray curves at $\eta = 1$ indicates supersymmetry.

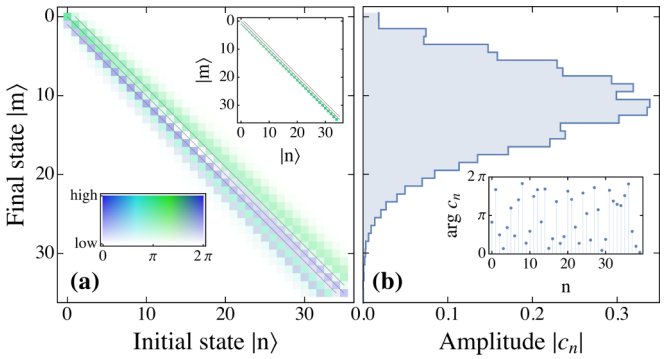

FIG. 8. (a) Matrix elements in the Fock basis of the shaking process $V(x,t) = V_{\rm osc}[x + x(t)]$ using the optimal shaking parameters in the first path, $\delta_x\sigma_t = 0.0470\,x_0 \times 2\pi/\omega$, and $\phi = 0.06\pi$. Inset: Matrix elements of the harmonic creation operator $\hat{B}^\dagger = \sqrt{n+1}|n+1\rangle\langle n|$. (b) Fourier coefficients of a typical desired state, $c_n = \langle n|\psi^{(1)}(t)\rangle$, in amplitude and phase. Within the corresponding energy range, we find satisfactory agreement of the two operators shown in (a).

$\chi_0(x)$ to any state $\chi_m(x)$ is given by

$$T_{m0} = \frac{T_{00}}{\sqrt{m!}}(iC^*)^m, \tag{D1}$$

where

$$C = \sqrt{\frac{2}{\pi}}\frac{\omega}{x_0}\int_0^T x(t)dt \approx -i\frac{\omega}{x_0}\delta_x\sigma_t e^{i\phi} \tag{D2}$$

for $2\omega^2\sigma_t^2 \gg 1$ and $t_0 \gg \sqrt{2}\sigma_t$. Note that this result depends only on the product $\delta_x\sigma_t$ and the phase ϕ.

We apply a shaking process $x^{(2)}(t)$ in the second path, starting from the ground state $\chi_0(x)$, to create a superposition of the ground state and the first excited state, $\zeta_0\chi_0(x) + \zeta_1\chi_1(x)$. To create this superposition we demand that $T_{00} = \zeta_0$ and $T_{10} \approx \zeta_1$. Since $\zeta_0^2 = \bar{x}^2/(\bar{x}^2 + 2x_0^2)$, as given in the main text, is close to unity for $\bar{x}/x_0 \gg 1$, we expect the transition probabilities to higher excited states with $m > 1$ to be negligible.

The shaking process conserves the norm, $\sum_{m=0}^\infty |T_{m0}|^2 = 1$, so it follows that $|C| = \sqrt{\ln|T_{00}|^{-2}}$. Using the assumption $T_{00} = \zeta_0$ and Eq. (D2), we find the correct shaking amplitude, that is,

$$\delta_x\sigma_t = \sqrt{\ln|\zeta_0|^{-2}} = \sqrt{\ln\left(1 + 2\frac{x_0^2}{\bar{x}^2}\right)}\frac{x_0}{\omega}. \tag{D3}$$

All other matrix elements are now given by Eq. (D1), in particular,

$$T_{10} = iT_{00}C^* = -\frac{1}{\sqrt{2}}\zeta_0\delta_x\sigma_t e^{-i\phi}. \tag{D4}$$

Since we aim at $T_{10} = \zeta_1 \geqslant 0$, where ζ_1 is real, this relation sets the correct amplitude relation to be $\phi = \pi$. We estimate the error ϵ of our ansatz by the sum of all higher excitation amplitudes, that is, $\epsilon = 1 - |T_{00}|^2 - |T_{10}|^2 \approx 2x_0^4/\bar{x}^4$.

With our choice of $\bar{x} = -5\,x_0$ the theoretical amplitude is $\delta_x\sigma_t = 0.0442\,x_0 \times 2\pi/\omega$, which is in excellent agreement with our numerical optimized result $\delta_x\sigma_t = 0.046\,x_0 \times 2\pi/\omega$.

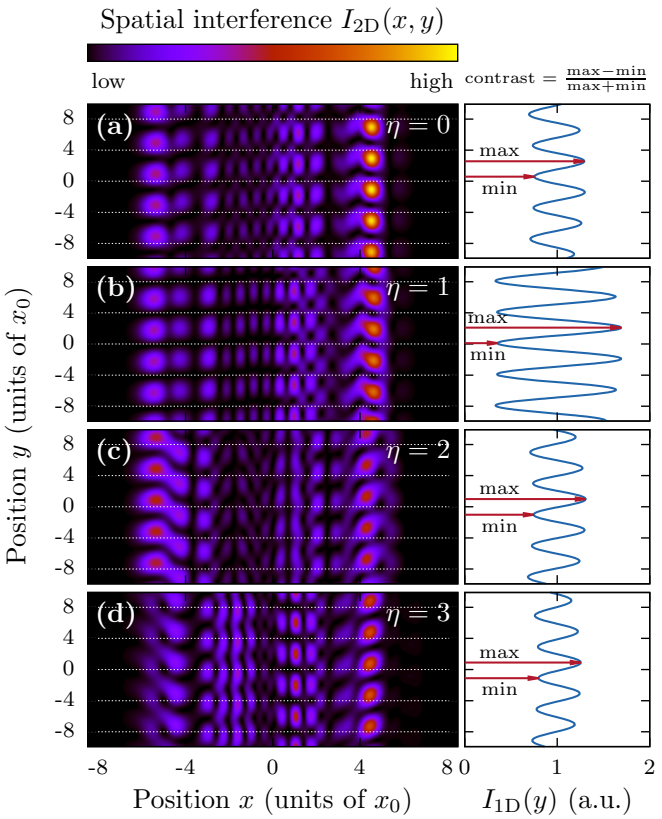

FIG. 9. Interference pattern $I_{2D}(x,y)$ for a hold time $t_r = 4 \times 2\pi/\omega$ (color plot). Parallel interference fringes in the x direction indicate supersymmetry in the two paths. White dashed lines serve as guides to the eye. Integrating over the x axis gives a one-dimensional interference pattern $I_{1D}(y)$, from which we obtain its contrast. (a) $\eta = 0$ corresponds to identical potentials in both paths. (b) $\eta = 1$ is the supersymmetric case. (c) and (d) $\eta = 2,3$ show nonsupersymmetric cases.

The phase can be reproduced numerically exactly, $\phi = 1.00\pi$. The error estimate of the ansatz is $\epsilon = 3.2 \times 10^{-3}$.

In the second step, we apply a shaking process in the first path $x^{(1)}(t)$ to an unknown state $\psi^{(1)}(t_1)$. Numerically, we find the optimal amplitude relation to be $\delta_x \sigma_t = 0.0470\, x_0 \times 2\pi/\omega$. The numerical phase is $\phi = 0.06\pi$, while the phase dependency is weakened compared to the first case. In Fig. 8 we compare the matrix elements T_{mn} using these optimal shaking parameters with the operator $\hat{B}^\dagger$ at an energy range of a typical desired wave function.

APPENDIX E: INTERFERENCE PATTERN AND CONTRAST

For a realization with two spatially separated systems, the confining potentials are turned off to realize the second beam splitter. The two states, $\psi_f^{(1)}$ and $\psi_{f,\eta}^{(2)}$, expand rapidly in the y direction and form a two-dimensional interference pattern $I_{2D}(x,y)$ with interference fringes along the x axis [17,28–30] (see Fig. 9). The envelope of the pattern will depend on x and reflects the spatial density of the states in this direction. In the case of supersymmetry, the output states are equal up to a relative phase, $\psi_f^{(1)}(x) \sim \psi_{f,\eta}^{(2)}(x)$, and the fringes are perfectly parallel to the x axis.

We evaluate the two-dimensional interference pattern $I_{2D}(x,y)$ by integrating it over the full x axis, that is,

$$I_{1D}(y) = \langle\psi_f^{(1)}|\psi_f^{(1)}\rangle + \langle\psi_{f,\eta}^{(2)}|\psi_{f,\eta}^{(2)}\rangle + 2\left|\langle\psi_f^{(1)}|\psi_{f,\eta}^{(2)}\rangle\right| \cos\xi(y), \tag{E1}$$

where we use the shorthand notation $\langle\cdot|\cdot\rangle = \int_{\mathbb{R}} |\cdot|^2 dx$. The phase $\xi(y)$ is the argument of $\langle\psi_f^{(1)}|\psi_{f,\eta}^{(2)}\rangle$ and a linear function in y. The result $I_{1D}(y)$ is a one-dimensional interference pattern. For long enough expansion times, we can assume all terms $\langle\cdot|\cdot\rangle$ to be independent of y.

The contrast $\mathcal{C}$ of $I_{1D}(y)$ is defined by the maximum, $\max = \langle\psi_f^{(1)}|\psi_f^{(1)}\rangle + \langle\psi_{f,\eta}^{(2)}|\psi_{f,\eta}^{(2)}\rangle + 2|\langle\psi_f^{(1)}|\psi_{f,\eta}^{(2)}\rangle|$, and the minimum, $\min = \langle\psi_f^{(1)}|\psi_f^{(1)}\rangle + \langle\psi_{f,\eta}^{(2)}|\psi_{f,\eta}^{(2)}\rangle - 2|\langle\psi_f^{(1)}|\psi_{f,\eta}^{(2)}\rangle|$, in the following manner:

$$\mathcal{C} = \frac{\max - \min}{\max + \min} = \frac{2\left|\langle\psi_f^{(1)}|\psi_{f,\eta}^{(2)}\rangle\right|}{\langle\psi_f^{(1)}|\psi_f^{(1)}\rangle + \langle\psi_{f,\eta}^{(2)}|\psi_{f,\eta}^{(2)}\rangle}. \tag{E2}$$

The contrast is 1 if the two states are equal up to a relative phase. This holds for supersymmetric partner potentials for any initial state ψ_i and any time t_1. Otherwise, the contrast is smaller than 1 and is determined by fluctuating correlations also in nonsupersymmetric cases, resulting in a residual contrast.

In the numerical simulations, we do not consider the expansion in the y direction. Instead, we directly evaluate the second expression of Eq. (E2).

APPENDIX F: ON THE DISPLACEMENT $\bar{x}$

In our proposal we initialize the system by displacing the ground state of the harmonic confinement by $\bar{x}$. On the one hand, a large displacement improves the initialization process in the second path of the interferometer [see Fig. 2(b)]. On the other hand, the correct potential shape, including harmonic confinement and localized central barrier, has to be ensured to energies of the order of $\hbar\omega(\bar{x}/x_0)^2/2 \propto \bar{x}^2$, which might constitute an experimental challenge that limits how large $\bar{x}$ can be chosen. In this paper, we choose $\bar{x} = -5\, x_0$ in our main example, which displays the desired effect. We have considered other values such as $\bar{x} = -3\, x_0$. Here, the contrast after the shaking pulse as depicted in Fig. 4(c) gives lower peaks at $\eta = \pm 1$ while the residual contrast away from $\eta = \pm 1$ is increased.

[1] E. Witten, Nucl. Phys. B **188**, 513 (1981).
[2] C. V. Sukumar, J. Phys. A **18**, 2917 (1985).
[3] F. Cooper, A. Khare, and U. Sukhatme, Phys. Rep. **251**, 267 (1995).

[4] E. Schrödinger, Proc. R. Ir. Acad., Sect. A **46**, 9 (1940).
[5] A. Valance, T. J. Morgan, and H. Bergeron, Am. J. Phys. **58**, 487 (1990).
[6] M. Bernstein and L. S. Brown, Phys. Rev. Lett. **52**, 1933 (1984).
[7] F. Marchesoni, P. Sodano, and M. Zannetti, Phys. Rev. Lett. **61**, 1143 (1988).
[8] C. V. Sukumar, J. Phys. A **19**, 2297 (1986).
[9] H. Fakhri, S. Sobhanian, and H. Zahed, New J. Phys. **4**, 55 (2002).
[10] A. del Campo, M. G. Boshier, and A. Saxena, Sci. Rep. **4**, 5274 (2014).
[11] J. Ulrich, D. Otten, and F. Hassler, Phys. Rev. B **92**, 245444 (2015).
[12] We use the indices ↑ and ↓ and 1 and 2 interchangeably.
[13] We note that the properties of these systems can also be obtained with the factorization method [3, 31], which is closely related.
[14] M. Atiyah, R. Bott, and V. K. Patodi, Invent. Math. **19**, 279 (1973).
[15] N. Berline, E. Metzler, and M. Vergne, *Heat Kernels and Dirac Operators* (Springer, Berlin, 2004).
[16] Synthetic gauge fields in ultracold-atom systems are reviewed in J. Dalibard, F. Gerbier, G. Juzeliunas, and P. Öhberg, Rev. Mod. Phys. **83**, 1523 (2011).
[17] S. Hofferberth, I. Lesanovsky, T. Schumm, A. Imambekov, V. Gritsev, E. Demler, and J. Schmiedmayer, Nat. Phys. **4**, 489 (2008).
[18] M. Reicherter, T. Haist, E. U. Wagemann, and H. J. Tiziani, Opt. Lett. **24**, 608 (1999).
[19] A. L. Gaunt and Z. Hadzibabic, Sci. Rep. **2**, 721 (2012).
[20] F. Nogrette, H. Labuhn, S. Ravets, D. Barredo, L. Béguin, A. Vernier, T. Lahaye, and A. Browaeys, Phys. Rev. X **4**, 021034 (2014).
[21] P. Zupancic, P. M. Preiss, R. Ma, A. Lukin, M. E. Tai, M. Rispoli, R. Islam, and M. Greiner, Opt. Express **24**, 13881 (2016).
[22] F. Serwane, G. Zürn, T. Lompe, T. B. Ottenstein, A. N. Wenz, and S. Jochim, Science **332**, 336 (2011).
[23] The transmission of the barrier is approximately $1/2$ for $A = \sqrt{1+\bar{x}^2/x_0^2}$, as we have checked numerically.
[24] $\eta = -1$ corresponds to replacing $V^{(2)}(x)$ by $V^{(2)}(-x)$, which is also a supersymmetric partner of $V^{(1)}$.
[25] M. Tomka, M. Pletyukhov, and V. Gritsev, Sci. Rep. **5**, 13097 (2015).
[26] I. B. Spielman, Phys. Rev. A **79**, 063613 (2009); Y.-J. Lin, R. L. Compton, K. J. Garcia, J. V. Porto, and I. B. Spielman, Nature (London) **462**, 628 (2009).
[27] R. P. Feynman and A. R. Hibbs, *Quantum Mechanics and Path Integrals* (McGraw-Hill, London, 1965), p. 232.
[28] M. R. Andrews, C. G. Townsend, H.-J. Miesner, D. S. Durfee, D. M. Kurn, and W. Ketterle, Science **275**, 637 (1997).
[29] A. Polkovnikov, E. Altman, and E. Demler, Proc. Natl. Acad. Sci. USA **103**, 6125 (2006).
[30] Z. Hadzibabic, P. Krüger, M. Cheneau, B. Battelier, and J. Dalibard, Nature (London) **441**, 1118 (2006).
[31] L. Infeld and T. E. Hull, Rev. Mod. Phys. **23**, 21 (1951).